Self-Focusing of Intense Laser Pulses in a Clustered Gas

I. Alexeev,[1] T. M. Antonsen,[2] K. Y. Kim,[1] and H. M. Milchberg[1]

[1]*Institute for Physical Science and Technology, University of Maryland, College Park, Maryland 20742*

[2]*Institute for Research in Electronics and Applied Physics, University of Maryland, College Park, Maryland 20742*

(Received 23 October 2002; published 10 March 2003)

We report the self-focusing of intense laser pulses in gases composed of atomic clusters. This is in strong contrast to beam spreading owing to ionization-induced refraction commonly observed in nonclustered gases. The effect is explained in terms of the ensemble average transient polarizability of the heated clusters as they explode in response to the intense pulse.

DOI: 10.1103/PhysRevLett.90.103402 PACS numbers: 36.40.Vz, 36.40.Gk, 52.38.Hb

The interaction of intense laser pulses with atomic clusters is an active area of research that has several promising applications, which include the generation of x rays [1], energetic electrons and ions [2], and nuclear particles [3]. The analysis in most of the work to date, even in experiments with high-density cluster jets, has focused on the dynamics of individual clusters in prescribed laser fields.

In this Letter, we present results revealing a strong macroscopic effect on laser beams owing to their interaction with a gas of clusters. In particular, a clustered gas can act as a positive lensing or guiding medium. This can occur at moderate pulse intensities below $\sim 10^{15}$ W/cm^2, so the effect is unrelated to either relativistic self-focusing or ponderomotive filamentation [4]. The effect stands in strong contrast to the well-known negative lensing or defocusing experienced by an intense pulse propagating in unclustered gases [5], where direct ionization by the laser field produces a local electron density profile peaked along the beam axis. Such a profile produces a radially increasing refractive index, which leads to pulse defocusing. Self-focusing in clustered gases may have played a role in many earlier experiments, leading to cluster interactions at higher intensities than previously suspected.

The self-focusing effect originates from the manner in which individual clusters heat up and explode in the presence of the laser pulse. We have found that the time variation of the complex cluster polarizability γ, where $\mathbf{p} = \gamma \mathbf{E}$ is the cluster dipole moment and $\mathbf{E}$ is the external laser field, embodies the details of the cluster dynamics. The temporal behavior of $\mathrm{Re}(\gamma) = \gamma_r$ for an individual cluster is determined by a competition in its optical response between the portion of its expanding plasma above critical density and the portion below: $\gamma_r > 0$ when the supercritical density material dominates the response, and $\gamma_r < 0$ when the subcritical density response dominates [6]. As the cluster is heated and expands, γ_r starts positive and initially increases with time [peaking at t_{peak}, say [see Fig. 1(a)]. It then decreases and crosses through zero, approaching asymptotic negative values $\gamma_{r,\mathrm{long}}$ for $t > t_{\mathrm{long}}$. For clusters near the beam center, where the intensity is high, γ_r rises faster than at the edge of the beam. The self-focusing effect is understood by considering the radial and time variation of the average polarizability $\bar{\gamma}$ over an ensemble of clusters in a gas. The result is a beam-axis-peaked radial profile of $\bar{\gamma}_r$ (or real index $n_r = 1 + 2\pi N_c \bar{\gamma}_r$, where N_c is the cluster number density) at early times which gives rise to pulse self-focusing.

These physical insights derive from our self-consistent laser-cluster interaction model, the full details of which can be found in Ref. [7]. The model calculates the transient complex polarizability of an expanding cluster for prescribed laser pulses. Figure 1(a) shows calculated radial profiles of $\mathrm{Re}(\bar{\gamma})$ and $\mathrm{Im}(\bar{\gamma})$ as functions of time in response to an 800 nm Gaussian pump pulse of peak intensity 5×10^{15} W/cm^2, 100 fs FWHM pulse width, and FWHM spot size of 15 μm. The ensemble average polarizability $\bar{\gamma}$ was calculated by using a weighted average result for a range of cluster sizes, simulating a gas with a 100% FWHM cluster size distribution [8] centered at 300 Å. The pump pulse envelope is overlaid on the plot for $\mathrm{Re}(\bar{\gamma})$. Thus, the pulse resides where $\bar{\gamma}_r$ decreases with radius and self-focusing is expected. The calculations show that for longer pulses, an increasing portion of the pulse envelope exists in the $\bar{\gamma}_r < 0$ region. There is also absorption, maximizing as $\mathrm{Im}(\bar{\gamma}) = \bar{\gamma}_i$ peaks near the zero crossing of $\bar{\gamma}_r$ (defined to be at $t = 0$ for later comparison with Fig. 4), and which falls off over a few hundred femtoseconds. For $t > t_{\mathrm{long}}$, $\bar{\gamma}_r(r = 0) \rightarrow \bar{\gamma}_{r,\mathrm{long}}$ [or $n_r(r = 0) \rightarrow n_{r,\mathrm{long}} = 1 + 2\pi N_c \bar{\gamma}_{r,\mathrm{long}}$], where $n_{r,\mathrm{long}}$ is the index of a locally *uniform* background plasma. This is so even though the evolution of $\bar{\gamma}_r$ to $\bar{\gamma}_{r,\mathrm{long}}$ occurs well before the plasmas from adjacent exploding clusters merge [6]. It is therefore expected that for pulses longer than t_{long}, little transient beam lensing will occur. The asymptotic polarizability $\bar{\gamma}_{r,\mathrm{long}}$ is reached quickly: $t_{\mathrm{long}} \sim 0.5$–1 ps, depending on average cluster size [6,7]. Using single-shot spectral interferometry measurements, we have recently experimentally verified our model of cluster polarizability [6].

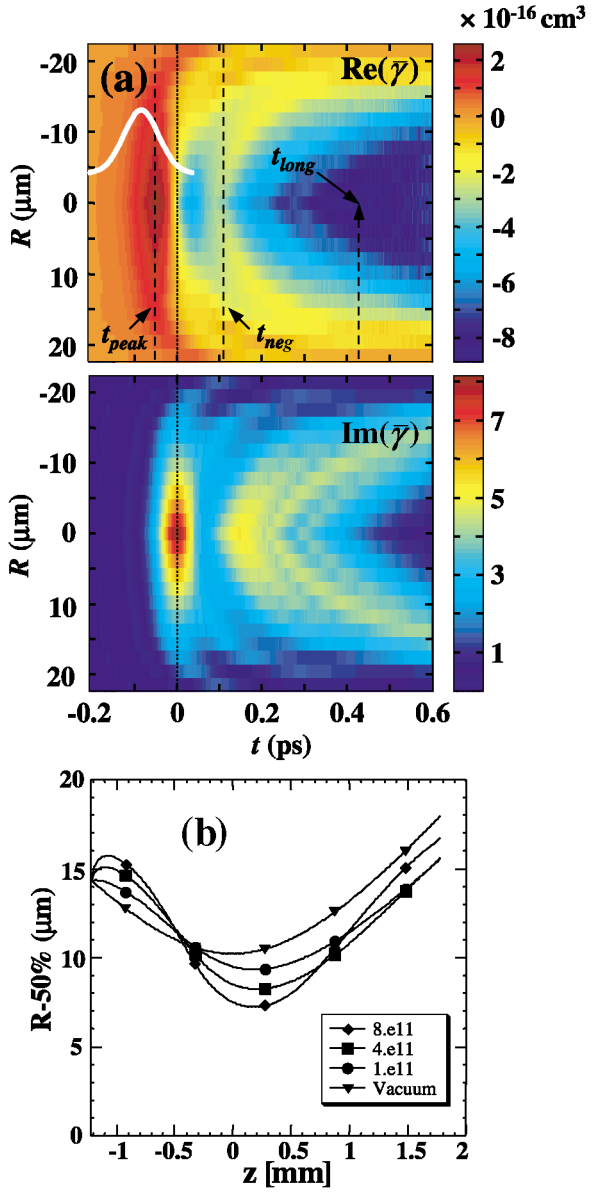

FIG. 1 (color). (a) Color scale plots of $\bar{\gamma}_r$ and $\bar{\gamma}_i$ versus radius and time calculated for a gas of 300 Å average radius clusters (with a 100% FWHM size distribution) heated by a 100 fs pulse of peak intensity 5×10^{15} W/cm^2 in a 15 μm FWHM spot. (b) Plots of radius through which 50% of the pulse energy reaching a distance z passes, for the same pulse as in (a) and several cluster densities N_c. In vacuum, the pulse focuses to a 15 μm FWHM spot size at $z = 0$.

To study the expected beam self-focusing, 7.5 mJ, 800 nm laser pulses in the range 80 fs–1.4 ps were focused at $f/12$ (spot FWHM = 15 μm, confocal parameter $2z_0 = 650$ μm, peak intensity 3.5×10^{16} W/cm^2) into an argon cluster jet backed at 400 psi. Pulse width variation (with positive chirp) was achieved by detuning the laser system's grating compressor. An average cluster radius of approximately 300 Å was estimated using the Hagena scaling based on our nozzle geometry and backing pressure [9]. The laser vacuum focus was located 0.5 mm before the jet center and 2 mm above the nozzle orifice. The full path of the beam through the jet was 3 mm. The effect of the cluster gas on beam propagation was diagnosed in multiple ways: the beam profile emerging at the gas jet exit was imaged, transverse interferograms and shadowgrams (phase sensitive images) were taken of the cluster plasma index profile induced by the pump beam propagation, and spectral interferometry [10] was performed using a probe beam copropagating with the pump.

Figure 2(a) shows a sequence of images of the beam at the jet exit as a function of laser pulse width τ. The mode diameter decreases to a minimum near $\tau \sim 350$ fs, and then increases again as the minimum pulse width is approached. Insets (i) and (ii) show, respectively, the root mean square exit beam radius $R_{\rm rms}$ and the pulse energy transmission fraction T as a function of pulse

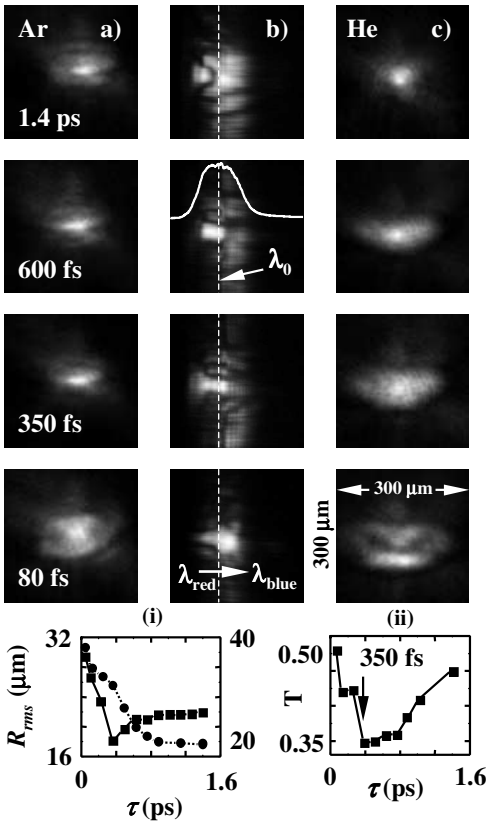

FIG. 2. (a) Image of pump beam at exit plane of Ar cluster jet versus pulse width. (b) 1D image slice of pump beam at exit plane of Ar cluster jet versus pump wavelength component. Vertical axis: beam spatial axis. Horizontal axis: wavelength. λ_0 = central wavelength. The pump pulse spectrum is superimposed on one of the panels as a white curve. (c) Image of pump beam at exit plane of He jet versus pulse width. Inset (i): Pump beam jet exit rms radius versus pulse width [argon cluster jet (squares and left scale); helium jet (circles and right scale)]. Inset (ii): Pump beam transmission through Ar cluster jet versus pulse width.

width. All points are 50 shot averages. The minimum in T at $\tau \sim 350$ fs is coincident with that in R_{rms}, with higher transmission at shorter and longer pulse widths. By contrast, Fig. 2(c) shows a sequence of exit beam images for 400 psi of helium, which does not cluster under these conditions, using the same jet, laser pulse energy, and focusing geometry. Here it is seen that the exit mode diameter decreases with increasing pulse width, as also shown with R_{rms} in inset (i). The result for helium is consistent with the mechanism of ionization-induced refraction in unclustered gases [5]. From interferometry, the peak average electron density for the He plasma is 10^{18} cm^{-3}; this is significantly lower than the 5×10^{18} cm^{-3} measured for the Ar cluster plasma. Remarkably, despite the higher electron density, the cluster plasma exhibits focusing rather than defocusing. For 300 Å argon clusters, the average electron density of 5×10^{18} cm^{-3} implies $N_c \sim 3 \times 10^{11}$ clusters/cm^3 for an average ionization of $Z \sim 10$ [6].

Because all pulses except for the minimum pulse width are positively chirped, examination of spectrally dispersed exit mode images allows assessment of dynamic beam lensing within the pulse envelope. The exit mode was imaged onto the entrance slit of a spectrometer, with the results shown in Fig. 2(b): 1D spatial slices of the exit mode versus wavelength. These images reveal that the mode images of Fig. 2(a) are actually composites. As the pulse is shortened, more and more of the spectrum is concentrated in a smaller exit mode, with the minimum spot occurring for $\tau \sim 350$ fs. As the pulse is shortened further to 80 fs, the exit mode expands for all spectral components.

We have also visualized the path of the propagating pump pulse by side probing the plasma left behind it. Figure 3 shows shadowgrams taken with a synchronous probe pulse that perpendicularly crosses the path of the pump just as it exits on the right (~ 10 ps after its entrance on the left). A diagram for a similar setup can be found in Ref. [11]. For $\tau = 1.4$ ps, the beam focus appears coincident with its vacuum location (indicated on figure), beyond which the pulse weakly diverges. As the pulse width is decreased, the profile near the beam waist becomes more constricted radially and the beam diverging beyond the waist begins to collimate. At $\tau =$ 350 fs, a weak secondary focus (indicated on image) appears beyond the first. By $\tau = 150$ fs, the beam appears to have strongly pinched down near its waist and then diverges more strongly on the other side. This trend continues down to $\tau = 80$ fs, where the post-focus divergence is even stronger. An interferogram is shown corresponding to the $\tau = 80$ fs shadowgram, where the fringe shift has become very small in the pinched waist region, but returns to appreciable levels on either side of it. This corresponds to a reduction in chordally integrated electron density near this waist, the cause of which is a greatly reduced local beam diameter consistent with self-focusing. The full range of images show roughly constant jet exit beam divergence for the pulse width range $\tau \sim$ 1.4 ps–550 fs and show a sharp increase for pulses shorter than $\tau \sim 350$ fs. This is consistent with the exit mode images of Figs. 2(a) and 2(b) and inset (i).

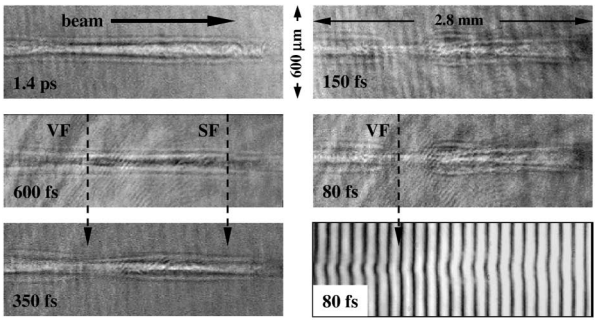

FIG. 3. Transverse shadowgraphs of pump beam track in cluster jet 10 ps after pump enters from left for selected pump pulse widths. VF: location of vacuum focus. SF: location of weak secondary focus. An interferogram is shown below its corresponding shadowgraph for the 80 fs pump pulse.

All of the above observations are explained by considering the self-focusing of the pump beam in the transient cluster plasma [see Fig. 1(a)]: Short pulses, here for $\tau <$ 350 fs, experience much of the positive profile of $\bar{\gamma}_r$ and self-focus. As a simple check that this is possible, we note that in order for the beam to overcome diffraction and self-focus, the index variation across the beam should be such that $\Delta n_r > \lambda/2\pi z_0$, or $N_c \bar{\gamma}_r^{\max} > \lambda/4\pi^2 z_0$. For our parameters ($N_c \sim 3 \times 10^{11}$ cm^{-3}, $\bar{\gamma}_r^{\max} \sim 2.5 \times 10^{-16}$ cm^3, $\lambda = 800$ nm, $z_0 = 325$ μm), this condition is easily satisfied. At longer times, once $\bar{\gamma}_r$ crosses below zero over the whole profile (for $t > t_{\mathrm{neg}}$, say [see Fig. 1(a)]), beam defocusing can occur, just as in an ordinary unclustered gas plasma. At intermediate times $t_{\mathrm{peak}} < t < t_{\mathrm{neg}}$, focusing or defocusing can occur depending on details of the transverse profile of $\bar{\gamma}_r$. For times $t >$ t_{long}, little further change in the n_r profile takes place as discussed above. Thus, it is expected that pulses with $\tau \sim$ 0.5–1.4 ps would have similar beam divergences, and this is what is observed in Fig. 2 [see especially inset (i)] and Fig. 3.

Simulations of pulse propagation in rapidly evolving clustered gases were conducted using a modified version of the electromagnetic propagation code WAKE [12]. The complex $\gamma(t)$ of a single cluster was computed using our laser-cluster interaction model [7] for the pulse durations of interest and for a range of peak intensities. This was used to construct a temporal and radial profile of the complex dielectric response of the cluster plasma, which was imported into WAKE to simulate pulse propagation in this dynamic medium. We note that these pulses merely sample the medium, as would a weak probe pulse. Figure 1(b) shows the results of simulations for a 100 fs pulse for varying cluster number density N_c. Plotted is the

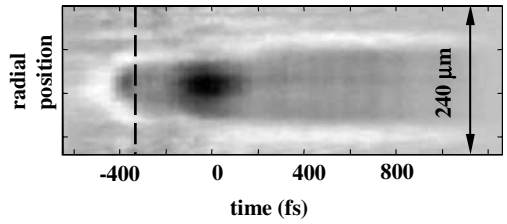

FIG. 4. Probe beam intensity versus transverse position and time derived from spectral interferometry. The pump pulse was 80 fs FWHM with peak intensity of 10^{15} W/cm^2. The vertical dashed line indicates the location of the pump pulse peak.

radius through which 50% of the pulse energy reaching a distance z passes. It can be seen from the plots that the minimum spot size decreases with increasing N_c while the output angular divergence increases, indicating that the cluster plasma is focusing the pulse. The calculation predicts a strong effect at our estimated $N_c \sim 3 \times 10^{11}$ cm^{-3}. For higher N_c there is an initial transient increase in radius at the left of the plot that does not correspond to beam refraction, but rather results from the absorption of power near the beam axis at the end of the pulse.

The measurements of Figs. 2 and 3 highlight the effect of the pump pulse on itself. We have also measured the effect of 80-fs pump-induced cluster dynamics on a weak copropagating probe pulse. The idea here was to isolate the transient lensing effect induced by the evolution of nearly impulse-heated clusters. Our method of supercontinuum spectral interferometry [10] was used, in which refractive index transients up to ~1.5 ps long can be extracted with ~15 fs time resolution. Diagrams of this setup can be found in Refs. [10,11]. Two weak, linearly chirped, 1.5 ps, $\lambda_0 \sim 700$ nm, $\Delta\lambda \sim 100$ nm bandwidth pulses were generated synchronous with the pump pulse. These pulses followed the same path as the pump through the focusing lens into the cluster jet, although they were focused to a much larger vacuum spot size (~ 150 μm FWHM). The time- and 1D space-dependent phase and intensity profiles of the probe pulse exiting the jet were extracted using Fourier techniques [10,13]. The transient intensity profile is shown in Fig. 4. Earlier than ~ -400 fs, the clusters are not yet ionized, and there is no phase or intensity perturbation on the probe. Past ~ -400 fs, a radially widening intensity reduction of the probe begins (onset of pump-heated cluster absorption of the probe), which forms an effective beam diameter. We take the onset of Ar ionization (at $\sim 10^{14}$ W/cm^2 [14]) to occur at ~ -400 fs. This sets the location of the pump pulse peak as indicated by the vertical dashed line. The white boundary is caused by interference between the periphery of the phase-shifted part of the probe beam (which propagates through the exploding cluster gas) and the unshifted part, which does not encounter the heated clusters. This beam diameter then abruptly increases over a ~300 fs interval around $t = 0$. There is a strong reduction in beam intensity during this interval. These results are consistent with our model for the cluster transient polarizability [see Fig. 1(a)]: At early times, a positive profile in $\bar{\gamma}_r$ restrains probe beam divergence. During the ~300 fs interval around $t = 0$, $\bar{\gamma}_r$ changes sign and the disturbed portion of the probe exit beam increases in size. Finally, and convincingly, the strong enhancement in absorption over the beam size-change interval is consistent with the maximum in $\bar{\gamma}_i$ reached during the sign change of $\bar{\gamma}_r$. This is consistent with the minimum beam transmission for $\tau \sim 350$ fs pulses shown in inset (ii) of Fig. 2.

In conclusion, we have found that gases of atomic clusters can promote laser pulse self-focusing at intensities which are modest compared to those required for relativistic and ponderomotive self-focusing. Self-focusing in cluster targets may in fact be a routine occurrence in many experiments. The effect derives from the evolution of the transient cluster polarizability induced by the pulse. Our hydrodynamic model of individual cluster evolution explains the origin of this macroscopic beam effect.

This work is supported by the U.S. Department of Energy and the National Science Foundation. The authors thank E. Parra for help with the cluster jet.

[1] A. McPherson *et al.*, Phys. Rev. Lett. **72**, 1810 (1994).
[2] Y. L. Shao *et al.*, Phys. Rev. Lett. **77**, 3343 (1996); V. Kumarappan *et al.*, *ibid.* **87**, 085005 (2001); M. Lezius *et al.*, *ibid.* **80**, 261 (1998).
[3] T. Ditmire *et al.*, Nature (London) **398**, 489 (1999).
[4] C. E. Max, J. Arons, and A. B. Langdon, Phys. Rev. Lett. **33**, 209 (1974); J. Fuchs *et al.*, *ibid.* **80**, 1658 (1998); P. E. Young *et al.*, *ibid.* **75**, 1082 (1995); K. Krushelnick *et al.*, *ibid.* **78**, 4047 (1997).
[5] P. Chessa *et al.*, Phys. Rev. Lett. **82**, 552 (1999); S. Nikitin *et al.*, Opt. Commun. **157**, 139 (1998).
[6] K. Y. Kim, I. Alexeev, E. Parra, and H. M. Milchberg, Phys. Rev. Lett. **90**, 023401 (2003).
[7] H. M. Milchberg, S. J. McNaught, and E. Parra, Phys. Rev. E **64**, 056402 (2001).
[8] K. J. Mendham *et al.*, Phys. Rev. A **64**, 055201 (2001).
[9] E. Parra *et al.*, Phys. Rev. E **62**, R5931 (2000); O. F. Hagena and W. Obert, J. Chem. Phys. **56**, 1793 (1972); O. Hagena, Rev. Sci. Instrum. **63**, 2374 (1992).
[10] K. Y. Kim, I. Alexeev, and H. M. Milchberg, Appl. Phys. Lett. **81**, 4124 (2002).
[11] I. Alexeev, K. Y. Kim, and H. M. Milchberg, Phys. Rev. Lett. **88**, 073901 (2002).
[12] P. Mora and T. M. Antonsen, Jr., Phys. Plasmas **4** , 217 (1997).
[13] M. Takeda, H. Ina, and S. Kobayashi, J. Opt. Soc. Am. **72**, 156 (1982).
[14] S. Augst *et al.*, Phys. Rev. Lett. **63**, 2212 (1989).